Soft Matter

PAPER

View Article Online
View Journal | View Issue

Cite this: *Soft Matter*, 2014, **10**, 348

Role of microscopic phase separation in gelation of aqueous gelatin solutions

Damjan Pelc,[a] Sanjin Marion,[b] Miroslav Požek[a] and Mario Basletić*[a]

Received 30th September 2013
Accepted 29th October 2013

DOI: 10.1039/c3sm52542b

www.rsc.org/softmatter

Using a unique home-made cell for four-contact impedance spectroscopy of conductive liquid samples, we establish the existence of two low frequency conductivity relaxations in aqueous solutions of gelatin, in both liquid and gel states. A comparison with diffusion measurements using pulsed field gradient NMR, and circular dichroism spectroscopy, shows that the faster relaxation process is due to gelatin macromolecule self-diffusion. This single molecule diffusion is mostly insensitive to the macroscopic state of the sample, implying that we have a clear separation of gelatin molecules into a free and network-bound phase. Scaling relationships for the self-diffusion indicate that the gelation process is not a percolative phenomenon, but is caused by aggregation of triple helices into a system-spanning fibre network.

1 Introduction

Gels are solutions where a small fraction of a dissolved gelling agent controls the phase of the whole system.[1] Upon gelation, the molecules of the gelling agent form a network which spans the entire solution, making it solid-like. Several microscopic mechanisms can lead to the formation of such a network, from strong covalent bonding between gelator molecules to weak hydrogen or ionic bonds. The physics of weakly bound gels is of special relevance because the energy scale of intermolecular bonding approaches the thermal energy for temperatures close to room temperature. This makes gels thermoreversible – they can melt and gel repeatedly upon changing the temperature – with a gelation temperature $T_g \sim 300$ K. In this paper we study a well-known thermoreversible gelling system – aqueous solutions of gelatin – for which the gelation mechanism is still not completely understood, mainly because of the several time- and length-scales involved. While at temperatures much higher than T_g gelatin molecules are *random coils*; it is known that upon cooling they locally order to form helical segments.[2] These helices can connect up to three different gelatin molecules and play a crucial role in the gelation process, but still no consensus exists on the exact nature of gelation. Two models[3] seek to describe the formation of a gel network: (a) bond percolation[1,4] where the gel forms when the number of intermolecular connections (helical segments) exceeds a threshold value and a single cluster is created and (b) aggregation[5,6] where helices first aggregate into fibres, which then form a network. Recently, several compelling experimental studies showed that the widely accepted percolation scenario, within its two mean-field approaches (Flory-Huggins and Stockmayer theories),[7] cannot establish a clear connection between gel macroscopic and microscopic properties[8,9] nor explain glass-like dynamics.[5,6]

In order to resolve these issues, we examine the mesoscopic dynamics of gelatin molecules using three complementary experimental methods: low-frequency conductivity spectroscopy[10] and NMR diffusometry (pulsed-field-gradient, PFG NMR), and combine them with a microscopic probe, circular dichroism spectroscopy. The advantage of our transport experiments (conductivity spectroscopy) is that it probes the characteristic length scales above 1 μm, which is typically difficult to probe using light scattering methods. Furthermore, we introduce an improved four-contact setup for impedance spectroscopy, which eliminates electrode polarization problems. By using PFG-NMR we avoid difficulties encountered in dynamic light scattering (DLS), where the contribution from the arrested gel network can cause inconsistencies in results of diffusivity studies.[11–18] We are thus able to detect the macromolecular contribution to both conductivity and diffusion, obtaining unique insight into the dynamics of the gelatin molecules. Our results show that free and network-bound gelatin molecules are clearly dynamically distinct, and that single-molecule diffusion of the free molecules is essentially insensitive to the macroscopic state of the system. This is not expected for a simple scale-free percolation cluster and suggests that the gel structure forms by aggregation of gelatin molecules into larger, more rigid and possibly glassy bundles.

2 Experimental methods

2.1 Materials

Gelatin is a water soluble polypeptide[4,19] made by denaturation from collagen, an irreversible process that destroys one collagen molecule creating three gelatin strands. At low temperatures ($T < T_g$) it forms homogeneous and transparent thermoreversible

[a]*Department of Physics, Faculty of Science, University of Zagreb, Bijenička 32, 10000 Zagreb, Croatia. E-mail: basletic@phy.hr*

[b]*Institute of Physics, Bijenička 46, 10000 Zagreb, Croatia*

(weak) gels (*gel* state).[2] Above T_g the solution behaves as a viscous liquid (*sol* state). The sample used in this work is pig skin gelatin (Sigma-Aldrich, type A, Bloom 300, molecular mass ~50 kDa corresponding to ~300 monomers). Solutions were prepared by dissolving gelatin in MilliQ water and stirring at 60 °C for 2 hours, erasing any thermal memory. The sample volume was typically 75 μl for impedance spectroscopy and 17 μl for NMR measurements. Gelatin concentrations were between the minimum gelling concentration $c_g \approx 5$ g l^{-1} and ≈150 g l^{-1}, covering two regimes: *dilute* below the overlap concentration $c^* \approx 25$ g l^{-1} and *semi-dilute* above. Gelation is a slow kinetic process – it is impossible to stop the system at an intermediate step and measure dynamics. Thus, we did all measurements after a quench and wait time (non-equilibrium measurements)[13] to minimize the long length scale structural relaxations but still obtain systematic gelation.[4] Temperature-dependent measurements were done adhering to a strict protocol: a quench (5 K s^{-1}) from 50 °C to 5 °C; after waiting for 1 hour for the gelatin to renaturate and relax,[4,20] the temperature was raised after equilibration every 15 min and a measurement was performed. All data shown in this work are, except when noted differently, given for 10 °C (gel state) and for 42 °C (sol state), well away from the temperature range needed for full denaturation/renaturation of triple helices.[4,6,20]

2.2 Impedance spectroscopy

Gelatin is a weak polyelectrolyte with a net negative charge of several percent of the number of monomeric units.[21] Our samples thus consist of weakly charged gelatin molecules, dissociated counterions, and any excess salt contained in the sample, and the motion of the macromolecules can be investigated if one measures their contribution to the conductivity of the solution. Microscopically, we can treat the large gelatin molecules as Brownian particles and use the corresponding equation of motion (Langevin equation) to obtain a Drude-like contribution to the frequency dependent conductivity, $\hat{\sigma}(\omega) = \Delta\sigma/(1 + i\omega\tau)$.[22] This relaxation has the same form as a Debye relaxation in $\hat{\varepsilon}(\omega)$. By determining the conductivity spectra $\sigma(\omega)$, we can study the dependence of the relaxation time τ on the concentration and state of the sample.

We measure the impedance spectra of gelatin solutions in a planar four-contact arrangement, effectively eliminating electrode polarization artifacts.[10] Our approach is similar to dielectric spectroscopy, with the difference that in a given frequency range we detect the response of free charges, as opposed to bound charges (*e.g.* dipoles). Thus the appropriate response function is conductivity $\sigma(\omega)$ instead of permittivity $\varepsilon(\omega)$. Fig. 1 shows (typical) measured spectra of 85 g l^{-1} gelatin solution. We note two contributions to the conductivity relaxation: slow and fast. This is in contrast to other impedance spectroscopy results made with two-contact impedance cells (frequency range 1 Hz to 10 MHz),[24,25] where the low frequency contribution to impedance is screened by the (unwanted) electrode polarization effects. Electrode polarization typically occurs in conductive liquid samples due to the formation of ionic layers on current-carrying electrodes, and the response of

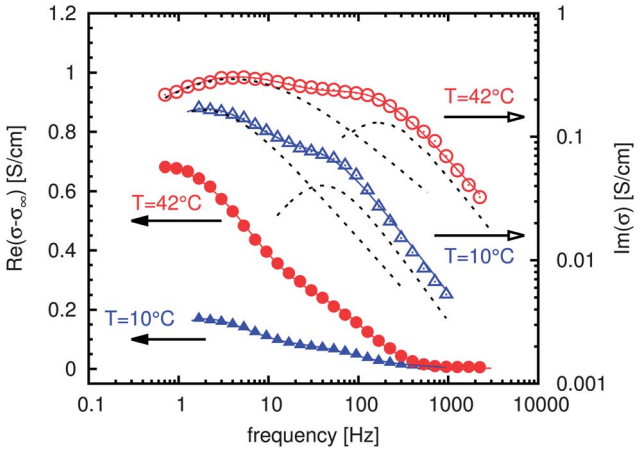

Fig. 1 Conductivity spectra of 85 g l^{-1} gelatin solution at 10 °C (triangles) and 42 °C (circles). Real (full symbols) and imaginary (empty symbols) parts of complex conductivity are shown. Solid lines: fits to two Cole–Cole relaxations.[23] Dotted lines: individual contributions of two relaxation processes in Im(σ).

the layers screens the response of the sample bulk. While other attempts to mitigate electrode polarization had limited success (see references within ref. 10), the four-contact technique enables voltage measurements to be done on separate electrodes with a high impedance instrument, thus eliminating current flow and the formation of charge layers on the voltage electrodes. This enabled us to measure a 'clean' response of the bulk material. Before measuring on gelatin samples, our custom-made four-contact setup[10] was tested with pure KCl water solutions, yielding flat spectra in the entire experimental frequency range and for several salt concentrations (for a detailed description of the testing procedure and results see ref. 10), establishing that it is an adequate tool for conductivity studies of liquid samples at low frequencies.

Impedance spectra were recorded for the entire concentration range, in both sol and gel states, and relaxation times were extracted. To include the possibility of a spread of characteristic time scales in each process, we analyze our data with the generalized form of the Debye (Drude) formula, the Cole–Cole[23] functional form for complex conductivity, with fast and slow relaxation processes:

$$\hat{\sigma}(\omega) = \sigma_\infty + \frac{\Delta\sigma_f}{1 + (i\omega\tau_f)^{\beta_f}} + \frac{\Delta\sigma_s}{1 + (i\omega\tau_s)^{\beta_s}}. \quad (1)$$

here $\tau_{f,s}$ are characteristic times, $\beta_{f,s}$ are exponents corresponding to the spread of relaxation times in the spectrum, $\Delta\sigma_{f,s}$ are contributions of (f)ast/(s)low processes to the total conductivity, and σ_∞ is the conductivity due to (small) counterions. Full lines in Fig. 1 show Cole–Cole fits to real and imaginary parts of the measured conductivity at fixed temperature, and dotted lines show two individual contributions, 'slow' and 'fast', to Im(σ). From the fits, we extract characteristic relaxation times $\tau_s \sim 1$ s and $\tau_f \sim 10$ ms. In this work we will focus on the fast relaxation process, which we show to be connected to macromolecular self-diffusion. The slow process is possibly connected with either retarded self-diffusion or cluster diffusion.

2.3 Pulsed field gradient NMR

To obtain additional information about the self-diffusion process we used PFG-NMR,[26] with a standard stimulated echo sequence.[27,28] This technique enables direct measurement of the dynamic structure factor $S(k, t)$ by spatially 'tagging' spins using magnetic field gradients (with a linear relationship between wavenumber k and gradient strength), and recording their position after a time t. Experiments were performed on hydrogen nuclei at 360 MHz using a Tecmag Apollo NMR spectrometer with a home-built gradient power supply and Oxford superconducting magnet, in a home-made NMR probe with gradient coils. Gradient strengths were from ~0.1 to ~1 T m^{-1}. The sample space of the gradient probe had a volume of only 17 μl, eliminating convection and inhomogeneous cooling/heating problems. PFG measurements were performed at a constant field gradient (wavenumber), measuring the decay of the stimulated echo in time (and compensating for spin-lattice relaxation). This was deemed more physical than the usual procedure of changing the gradient and keeping the diffusion time constant, as here one follows time evolution of the fluctuations on a given spatial scale, analogous to scattering methods. Although we were not able to make spectrally resolved diffusion measurements due to magnet homogeneity limitations, bulk water diffusion was clearly separable from macromolecule diffusion in the dynamic structure factor, and was visible as an additional contribution at short times (<5 ms). As water diffuses much faster than the macromolecules (and the gradient strengths employed were rather high), the water contribution is limited to short times and in most cases it decays to zero, long before the measurement window for gelatin diffusion (20 ms to 1 s) opens. Apart from the fast water contribution, dynamic structure factors $S(k, t)$ contain two contributions due to gelatin macromolecules (Fig. 2): a fast 'normal diffusion' part at times ~10 to 100 ms over long distances ($1/k$ ~ 1 to 10 μm), consistent with the conventional time and k dependence $S(k, t) \sim \exp(-k^2 D_f t)$ with an effective diffusion constant D_f, also observed in DLS studies;[12,13,29] and an anomalous, slow part at long times (~1 s). By comparison of the time-scales involved, we conclude that the last two contributions correspond to the relaxation processes observed in conductivity experiments. The effective diffusion coefficient for the fast process, D_f, is obtained directly from the short-time slope of ln S *vs.* t, as denoted in Fig. 2.

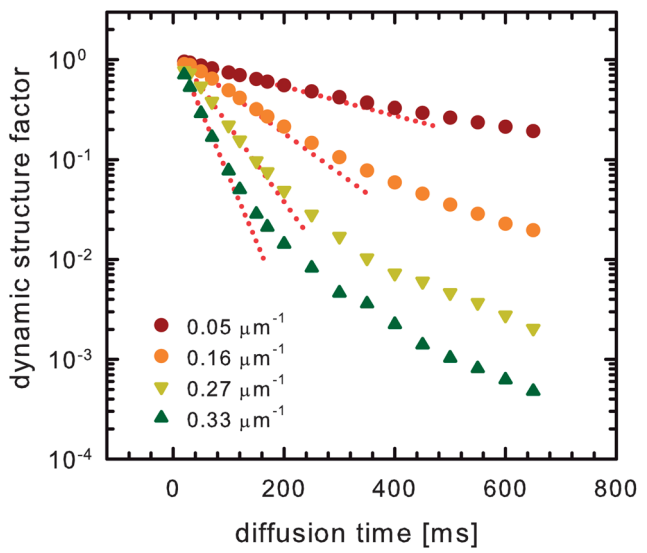

Fig. 2 Dynamic structure factor $S(k, t)$ from PFG NMR measurements, for gelatin solution concentration 15 g l^{-1} and at 15 °C. Two contributions from gelatin diffusion are clearly visible, while the bulk water contribution is shorter than 20 ms and thus outside the measurement window. The lines denote the slopes from which the effective diffusion coefficient D_f is calculated.

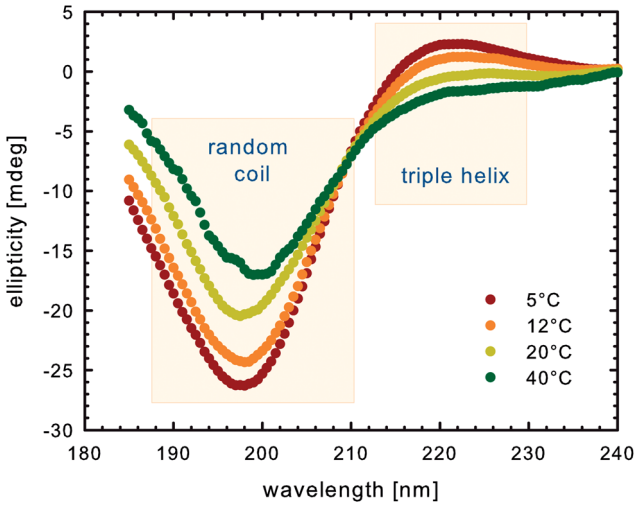

Fig. 3 Circular dichroism (CD) spectrum of a 1 g l^{-1} gelatin solution, at several temperatures. Two characteristic features are visible – the random coil region and the collagen triple helix region.

2.4 Circular dichroism spectroscopy

Circular dichroism (CD) spectroscopy in the far ultraviolet region is very sensitive to the secondary structure of proteins in solution,[30] so we used it to determine the concentration of triple helical segments in our gelatin samples. We used a Jasco J-815 CD spectrometer in the far UV range, with fast Peltier temperature control and a sample optical path of 0.1 mm, for CD measurements at several gelatin concentrations and temperatures. The CD spectra (2 g l^{-1} shown in Fig. 3) show two prominent features: a wide minimum centered around ~200 nm, characteristic of random coils, and, at lower temperatures, a smaller maximum centered at 221 nm, characteristic of collagen triple helices.[31] An isoelliptical point at 210 nm is also present at all temperatures, showing that the two contributions are well separated; this CD intensity was taken to be representative of the number of triple helical segments in all measured concentrations. Above concentrations of ~10 g l^{-1} it was difficult to record the entire spectra due to increased UV absorption below 210 nm, but no qualitative changes were observed in the spectra up to that concentration.

3 Results

3.1 Impedance spectroscopy

The dependence of fast conductivity relaxation time, from Cole–Cole fits, on the gelatin concentration c is shown in Fig. 4. In the dilute sol regime ($c < c^*$ and $T = 42$ °C) the relaxation time scales

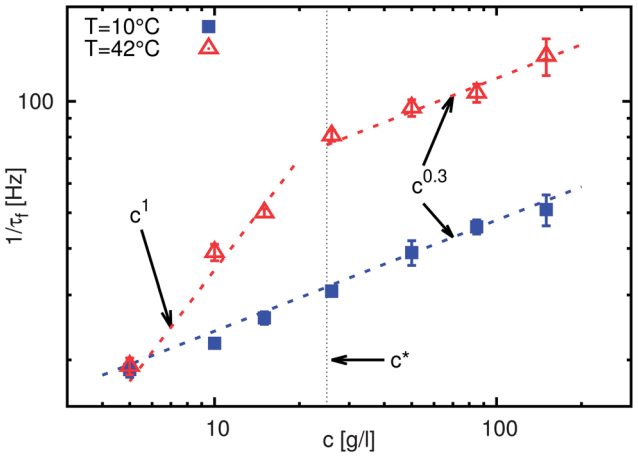

Fig. 4 Concentration scaling of inverse characteristic time τ_f for fast relaxation mode. Results are given for sol and gel states. $c^* = 25$ g l^{-1} corresponds to the crossover between dilute and semi-dilute regimes.

with c^{-1}, while in the semi-dilute sol regime ($c > c^*$) and all gel regimes ($T = 10$ °C) we obtain an unusual scaling of $\tau_f \sim c^{-0.3}$. We note that the relaxation is consistent with Debye relaxation, *i.e.* the exponent β_f is equal to 1 within experimental error, implying no local heterogeneities for the charge carrier environment. The nature of the relaxation and obtained exponents indicate that the fast relaxation can be interpreted as a conductivity contribution from self diffusion of gelatin molecules and any of their bound charges[32] – further confirmed with the NMR diffusiometry (see later). We note that without the information on the characteristic length scale L we cannot obtain the diffusion constant D, thus requiring the measurements of the diffusion constant at the same time scales *via* another experimental method (PFG NMR).

The dependence of effective diffusion constant D_f on the concentration, obtained from PFG-NMR and shown in Fig. 5, is also sensitive to the concentration regime. Below the overlap concentration c^*, the diffusion coefficient is essentially constant, as one might expect when molecular interactions are rare. Above c^*, D_f starts decreasing with increasing concentration. These trends are the same irrespective of the state of the sample, indicating that the local environment of (free) gelatin chains does not change significantly upon gelation. However, only upon combining the results of PFG-NMR and impedance spectroscopy we can obtain parameters insensitive to both the state and the concentration regime of the sample, providing quantitative information about the microscopic surrounding of the gelatin molecules.

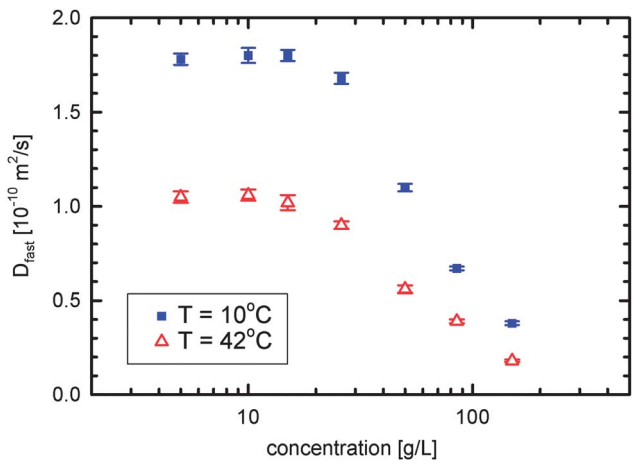

Fig. 5 Effective diffusion constant D_f as obtained from the dynamic structure factor measured by PFG-NMR, depending on the gelatin concentration.

3.2 Connecting diffusion and conductivity

Conductivity and PFG-NMR diffusion data can be put together to obtain a relationship between the concentration of charge carriers and dissolved gelatin. The Langevin equation approach provides a simple (Einstein) equation connecting the characteristic relaxation height $\Delta\sigma_f$ and the diffusion constant D_f with the effective number of charge carriers, n_f: $\Delta\sigma_f = n_f q_f^2 D_f / kT$ (see ref. 22) (q_f being the effective charge of carriers). As q_f is determined by the ionic environment of the gelatin, its concentration and temperature dependence is expected to be very weak in the studied range, so the quantity $n_f q_f^2$ can be taken as a direct measure of n_f, the number of mobile gelatin chains. We can now use values of $\Delta\sigma_f$ and D_f to obtain the concentration scaling of $n_f q_f^2$ (Fig. 6a). A scaling of the form $n_f q_f^2 \sim c^b$ is obtained with $b = (0.98 \pm 0.03)$ in the sol state and $b = (0.74 \pm 0.02)$ in the gel state. This scaling does not change at the transition concentration c^* between dilute and semi-dilute regimes; as the number of moving molecules is independent of concentration regime, this proves that we are indeed dealing with self-diffusion of gelatin molecules. The sol state scaling shows that there is a linear relationship between the number of charge carriers and the concentration of gelatin, as indeed one could expect,

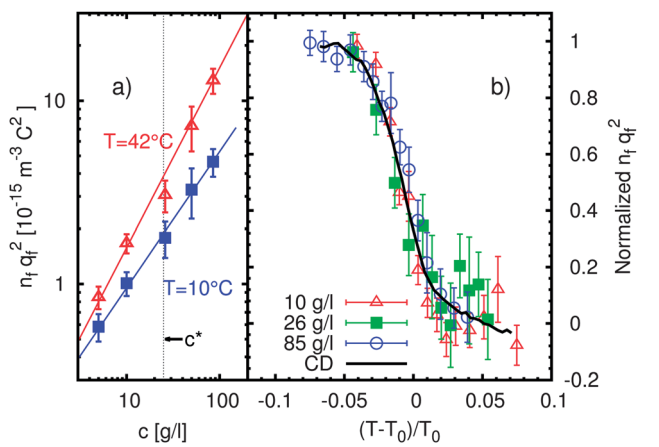

Fig. 6 (a) Quantity $n_f q_f^2$ obtained from diffusion and conductivity (see text). Lines: fits to $n_f q_f^2 \sim c^{0.98\pm0.03}$ for sol and $n_f q_f^2 \sim c^{0.74\pm0.02}$ for gel. (b) Temperature dependence of normalized numbers of gelatin molecules lost to the gel macrostructure ($n_f q_f^2$ for different concentrations were normalized to the same low and high temperature values). The full line is the master curve for the triple-helix formation obtained from circular dichroism (CD). T_0 is the transition temperature, which is different in self-diffusion (T_g) or circular dichroism (T_{CD}) (see text for details).

while in the gel state we lose a fraction of charge carriers due to gelation.

The numerical values for $n_f q_f^2$ for the case of ~100 monomeric units in our gelatin indicate that about 2–3% of monomers have dissociated, as would be expected for a weak polyelectrolyte. Symbols in Fig. 6b show the reduced temperature dependence of $n_f q_f^2$ normalized to high temperature values, for several concentrations. All data collapse on a master curve, with the point of inflection giving the gelation transition T_g as seen in self-diffusion, which is similar to the rheological transition temperature. Hence, molecular aggregation essentially progresses in much the same way for the entire studied concentration range. This universality goes down to the microscopic level: by using circular dichroism spectroscopy, we can gain insight into the helix dynamics at the molecular scales, and see that the aggregation process approximately follows this microscopic dynamics (full line in Fig. 6b).

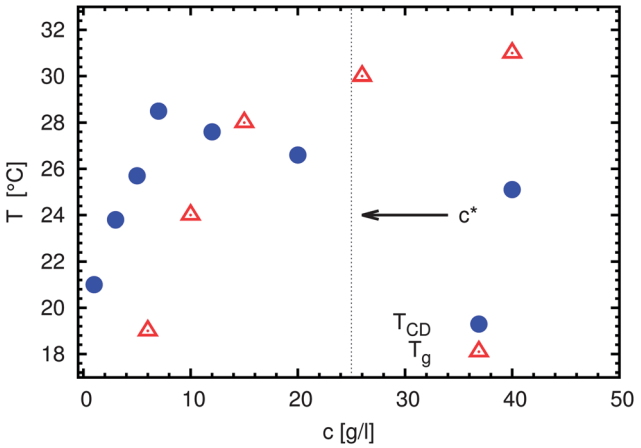

Fig. 7 Transition temperatures obtained as follows: T_g from self-diffusion (measures the sol–gel transition temperature; open triangles) and T_{CD} (measures the temperature for the formation of triple helices) as obtained from circular dichroism measurements (full circles).

3.3 Circular dichroism

Light polarization studies on gelatin[4,20,33,34] are able to follow the formation of helices as a function of temperature and concentration, and recent evidence shows that there exists a master curve for the concentration of triple helices in aqueous solutions of gelatin.[20] This confirms the notion that the triple-helix formation mechanism is independent of concentration. The full line in Fig. 6b shows one such master curve obtained by circular dichroism (CD) on our samples. The inflection point (midway in the curve) gives the temperature T_{CD} for the transition into triple-helices. This curve was obtained by using a reduced temperature $(T - T_{CD})/T_{CD}$ as observed in the conductivity data and by scaling the high and low temperature tails to the same asymptotic values. This CD curve shows the fraction of formed triple-helices as a function of temperature around the transition. Comparison with the conductivity data shows a temperature dependence similar to the number of molecules lost to the gel structure. Qualitatively one would expect such a connection, as helices act as intermolecular junctions. As we lower the temperature, first a sufficient number of triple-helices is formed before we can undergo the sol–gel transition. We note that for higher concentration results indicate that it is possible that sufficient triple-helices are formed before T_{CD} is reached. We emphasize that T_{CD} is the melting temperature for a single molecule, while T_g is the melting temperature of the whole gel network.

However, the concentration dependence of the transition temperature obtained from CD follows the crossover between two regimes:[33] at low concentrations (dilute) triple-helices form by the formation of single looped helices and at higher concentrations when entering the semi-dilute region the dominant nucleation is through non-looped helices. This explains why the transition temperature is lower for dilute solutions: the energy for forming a looped helix is higher than that for a non-looped helix.[33] But, this does not explain why T_{CD} decreases as concentration c increases above ~8 g l^{-1}, as shown in Fig. 7.

We propose a simple model to explain the extrema seen in T_{CD}. At the transition temperature T_g there (barely) exists a gel network formed by overextended triple helices. Thus, we have a mesh of rigid rods where the pore size is roughly equal to the length L of a triple-helix, and the size of the triple helices should scale as $L \sim b^{-1/2}$ on the concentration of available triple helices b (rigid rod mesh size scaling).[1] Guo *et al.*[34] obtained the fraction of gelatin molecules x turned into triple-helices at the gel temperature (Fig. 12 from ref. 34) using rheo-optics measurements. Their explanation is that at lower concentration triple-helix formation is dominantly intra-molecular, so more gelatin is needed for the formation of one helix, while – at larger concentration – it is more efficient to form fewer but longer helices. We approximate their experimental curve for the concentration dependence of the triple-helix fraction x at T_g by $x(c) \sim \Delta x e^{-c/c_0} + x_0$, where $c_0 \approx 18$ g l^{-1}. Thus, the concentration of available triple helices is the concentration of gelatin times the fraction of gelatin in triple helices $b \approx cx(c)$ (we purposefully omit any pre-factor; but the most probable value is ≈ 2). The thus obtained triple-helix length $L(c)$ as a function of gelatin concentration c falls from a high value at low concentrations to a minimum at c_0, and then raises again for higher concentrations reaching a plateau (we can not extrapolate this function further). This minimum of length is close to the location of the maximum in $T_{CD}(c)$. Because entropy favours smaller molecules, we expect that shorter triple-helices will be more stable.

An attempt to quantify why smaller helices are more stable would be as follows. Usually one considers the Gibbs free energy for triple helix formation as $\Delta G = L(\Delta H - T\Delta S)$, where L is the triple helix length, ΔH is the experimental enthalpy change per unit of length, and ΔS is the entropy change per unit length. But, in this simple approximation we neglected the fact that helices of different lengths will not have the same entropy per length. We work upon this simplified framework by including that in a good solvent the entropy change is not proportional to L but to $L \times L^{1/5}$ (the additional factor comes from the Flory exponent in the Gaussian chain entropy[1]). So, what effect would a change of length have? If we consider a triple helix of length $l < L$ then the new Gibbs free energy is $\Delta G' = l[\Delta H - T\Delta S(l/L)^{1/5}]$. We now try to find the new melting temperature T by putting $\Delta G' = 0$. By using that

the original melting temperature $T_m = \Delta H/\Delta S$ we obtain the new melting temperature $T = T_m(Ll^{-1})^{1/5}$, which is higher than for a longer triple-helix. *E.g.*, for a 10% reduction in length, the new transition temperature is 5 degrees higher.

To summarize, we have found that at T_g there exists a concentration where the length of triple helices that form a gel network is minimal. This is because we have two opposing trends: at higher concentrations the relative amount of gelatin required to form a 3D rigid mesh of triple-helices reduces, thus requiring shorter helices; and at higher concentrations less gelatin is involved in forming the triple-helices used for gelation, favouring a longer length. Because smaller helices are more stable, we expect an increase in the helix melting temperature at this critical concentration. For a better model, additional effects need to be taken into account that influence the concentration dependence: the length of a looped and non-looped helix at the same temperature will not be the same[33] and – at higher concentrations when approaching the semi-dilute solutions – the approximative scaling $L \sim b^{-1/2}$ will not be applicable because of fibre formation.

In contrast, the temperature needed for the formation of the gel network T_g (as detected in the self-diffusion) is only a function of the available junction sites. Thus it increases with the concentration c of gelatin molecules, saturating when all the possible triple helices are formed. The reason that part of the gelatin molecules remains outside of the gel network can be attributed to the limited time for triple-helix nucleation (due to quenching). This limits the maximum percentage of gelatin converted into triple-helices trough nucleation processes to roughly 45%, which can depend also on other factors.[33]

3.4 Length scale for diffusion

We can obtain a characteristic length scale L associated with the self-diffusion process by using the well-known relationship for normal diffusion $L^2 \sim D_f\tau_f$ (see Fig. 8). The temperature dependence of L for two concentrations shown in the inset of Fig. 8 shows that it is a well defined length scale, roughly independent of temperature and thus of the macroscopic state. However, the dynamics leading to a well-defined L is markedly different for dilute and semi-dilute solutions. The behaviour of dilute solutions in the sol state ($c_g < c < c^*$, $T = 42$ °C) is consistent with a picture of diffusing independent swollen coils: the scaling $\tau_f \sim c^{-1}$ (Fig. 4) shows that the time between collisions is proportional to the available volume per molecule, and for the characteristic length we obtain $L^2 \sim c^{-0.85}$, comparable to the scaling expected for non-overlapping spheres $L^2 \sim c^{-2/3}$. The difference is probably due to the concentration-dependent swelling of the polymer[35] and/or interactions of the polymers with each other and with the surrounding medium. The value of D_f indicates a gyration radius for the swollen coils of $R_g \approx 20$ nm, which is consistent with a simple estimate $R_g \sim aN^{1/2} \sim 10$ nm (for the monomer length $a \sim 1$ nm and $N \sim 100$, valid for our gelatin molecules). Scaling for the dilute gel state ($c_g < c < c^*$, $T = 10$ °C) is not well defined, which we speculate is due to the complexity of the gel forming below the polymer overlap concentration. We speculate that this could be due to a competition between aggregation and percolation, *i.e.* percolation prefers longer bond units while the trend at higher concentrations is to form thicker bond units (Fig. 9).

In the semi-dilute sol and gel states ($c > c^*$) we believe we detect translational diffusion resulting from reptation of gelatin macromolecules. We find $L^2 \sim c^{-1.5}$, consistent with the scaling of mesh size from De Gennes theory of polymers in good solvents,[1,36] with the mesh size ~100 to 300 nm (slightly larger than that indicated previously[12,13,37]) DLS studies report an analogous mode having a scaling $D_f \sim c^{-1.75}$,[11,12] while our results indicate a lower value $D_f \sim c^{-1.2}$. Although in the case of reptation one would expect a non-Debye relaxation and anomalous diffusion in PFG-NMR, we emphasize that we are working at longer length-scales than DLS: at our length and time scales ($1/k \sim 1$–10 μm, $t \sim 10$ to 100 ms) the reptation dynamics renormalizes into the translational diffusion D_f of the gelatin molecule center of mass, as expected for reptation.[38] Both theory and our experimental data show that the corresponding characteristic length L scales as the mesh size for (non-charged) semi-dilute polymers. If we consider the gel state in the semi-dilute regime, we have the same length scaling and time dependence as those in the sol. We thus conclude that self-diffusion must be independent of the macroscopic state of the sample, depending only on the existence of a polypeptide mesh, originating from either chain overlap or gelation. The length scale concentration dependence defining a mesh is almost unchanged above and below T_g.

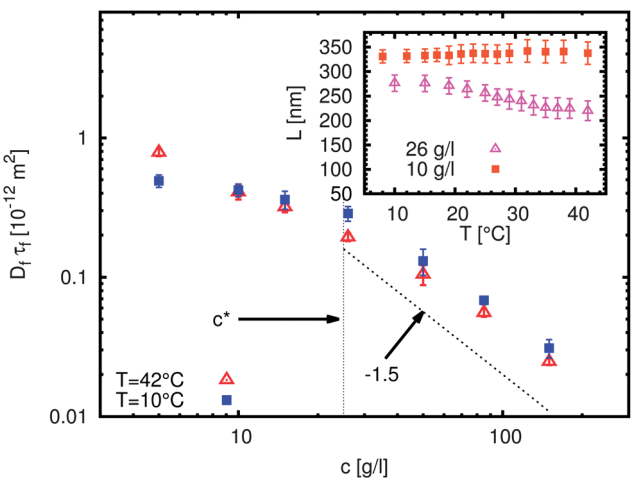

Fig. 8 Concentration scaling of the characteristic length scale for self-diffusion $L^2 = D_f\tau_f$. For $c > c^* = 25$ g l^{-1} data are consistent with scaling $L^2 \sim c^{-1.5}$ for both the sol and gel. Below c^*, the exponent reduces to $L^2 \sim c^{-0.85}$ for the sol state, while for the gel state the scaling exponent is not well defined. Inset: characteristic length L as a function of temperature T.

4 Discussion

The concentration of non-bound gelatin, as implied by Fig. 6a and 8, is sufficient to initiate the formation of triple-helices, but no such effect is seen in self-diffusion. Combined with the insensitivity of self-diffusion to the macroscopic state, it indicates that after gelation we have two phases, one analogous to the sol phase but less concentrated and an aggregated phase of gelatin not

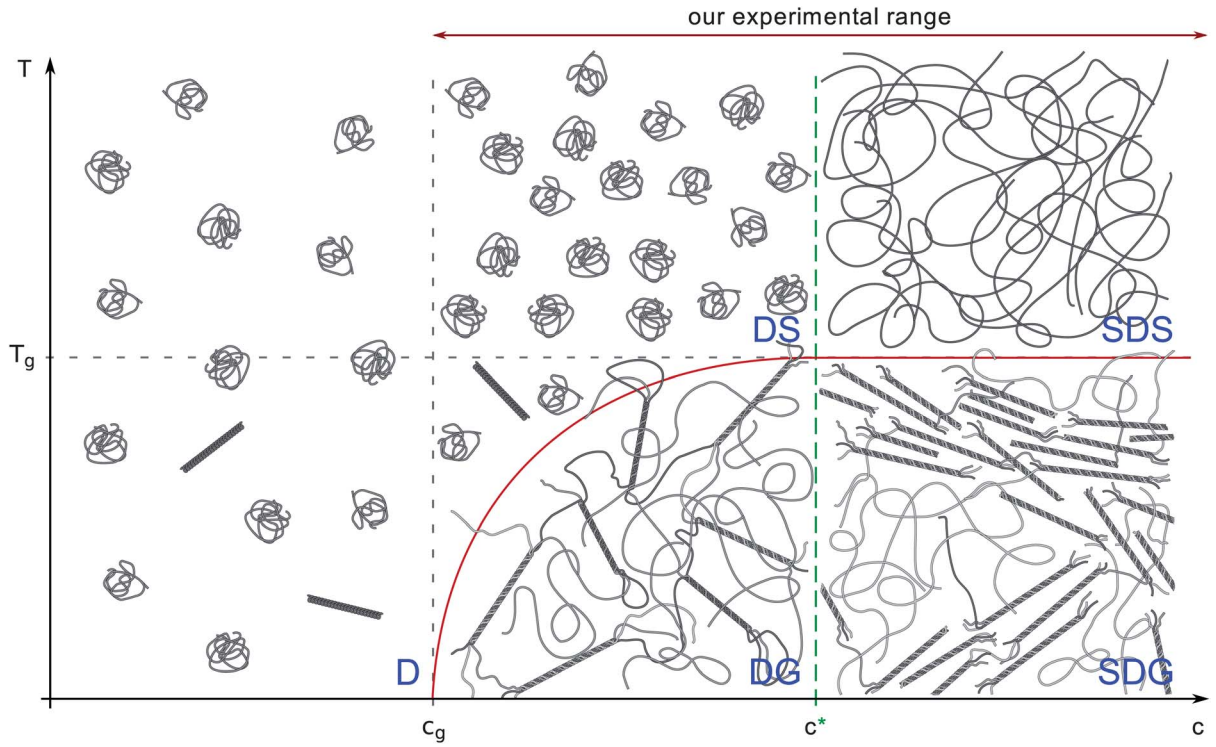

Fig. 9 Qualitative model of gelatin gelation mechanism based on our results and results from the existing literature. Below the minimum concentration for gelation, $c < c_g$ (not discussed here) we are in the dilute regime: there is no gel network. In the range $c < c < c^*$ we have two temperature regimes: the dilute-sol (DS), $T > T_g$, where the gelatin molecules exist as swollen random coils; and the dilute-gelling (DG) regime, $T < T_g$, where a gel network is formed due to the enlargement of the size of formed triple-helices. Above the overlap concentration c^* we have the semi-dilute sol regime (SDS) for $T > T_g$, while below T_g we have the semi-dilute gelling regime (SDG). Full (red) line denotes the boundary between sol (above) and gel (below) states. Note that we propose two different scenarios for gel network formation: the DG (percolation dominated) and SDG (aggregation dominated) scenarios.

contributing to transport. The formation of the gelatin gel by cooling the liquid phase can thus be imagined as follows (Fig. 9): a few kelvins above T_g helical segments start to appear on the gelatin molecules – this is a first-order transition on the level of single (or a few) chains. Helices typically involve three molecular strands, as this is the most stable configuration (a collagen-type triple helix). Due to the hydrophobicity of helical segments and attractive electrostatic interactions between them[39] they aggregate into fibre networks.[4,40,41] Since the molecules forming the fibres act as nucleation sites for further helix formation,[20] structures grow until an equilibrium macroscopic network is created – the gel. It is known that in a bad solvent (*e.g.* water–methanol) such emergent interactions lead to spinodal decomposition, but in pure aqueous dilute and semi-dilute solutions, there is no competition between gelation and precipitation because of the quality of solvent.[42,43] Thus the aggregation we observe can be regarded as a form of microphase separation distinct from spinodal decomposition.[1] A similar aggregation mechanism has recently been proposed by Ronsin *et al.*[44] for gelatin under shear. The network of aggregated fibres is responsible for macroscopic properties like elasticity, explaining why no simple correlation exists between the gel strength (macrostructure) and diffusivity of probe particles[9] and why microscopic probes like light scattering detect a different gelation transition point from macroscopic ones like rheology.[8]

As the gelation process was previously connected with percolation, current theories for similar systems do not account for the phase separation in the good solvent regime[35,45] due to neglected microscopic cooperativity. The available theories for thermoreversible gelation (see ref. 7 and 46–49) do not predict the concentration scaling for the diffusion and relaxation times nor the gelling behaviour in the dilute regime. Our results thus lead to the conclusion that gelatin is closer to systems showing phase separation with gelation like colloid gels[50] (*e.g.* continuum percolation) and similar systems.[51,52] One can also argue that the sol–gel transition in our system can be regarded as an 'ergodic–nonergodic' (phase) transition (dynamic arrest)[17,53] since the fibre network poses restrictions on thermal concentration fluctuations of gelatin. We suggest that there are similarities with glassy systems; we find the proposed analogy between triple-helix rods in a gelatin system and spins in a dilute magnetic spin-glass system (rod–glass transition)[54] striking. All these make gelatin an excellent system for studying the complex phenomena of fibre networks,[41,55,56] *e.g.* glassy behaviour under stress.[6]

5 Conclusion

In summary, by applying four-electrode impedance spectroscopy to dilute and semi-dilute gelling gelatin solutions we show

the existence of two processes that contribute to the frequency dependent conductivity. We identify the fast process as gelatin molecule self-diffusion due to long length scale reptation dynamics (translational diffusion). Self-diffusion at the cross-over from the dilute to semi-dilute state indicates that the microscopic diffusivity of particles is decoupled from the macroscopic properties of the gel. Due to a loss of charge carriers in the gel we argue that upon gelation two microphases exist in the system: the sol microphase with no interconnectivity and no difference from the sol macrophase and the fibre microphase formed *via* aggregation of triple-helices into fibre networks. Our results imply that semi-dilute (and dilute) gelatin solutions cannot be explained by simple percolation; we suggest that there are similarities with glassy systems. It is important to devise new methods to distinguish the true nature of the sol–gel transition. The similarity of rheological data between known fibre-formers (*e.g.* actin) and gelatin triple-helices[57] thus implies that gelatin is an interesting system for both studying the complex phenomena of fibre networks[41,55,56] and to benchmark thermoreversible gelation theories.

Acknowledgements

We are pleased to acknowledge the assistance of Nataša Šijaković-Vujičić and helpful discussions with Tomislav Vuletić. We thank Dr I. Piantanida for help with the CD measurements. We thank I. Delač Marion for producing some of the figures. The research leading to these results was supported by equipment financed from the European Community's Seventh Framework Programme (FP7/2007-2013) under grant agreement no. 229390 SOLeNeMaR, and by funding from the Croatian Ministry of Science, Education and Sports through grant no. 119-1191458-1023 and 119-1191458-1022.

References

1 P.-G. de Gennes, *Scaling Concepts in Polymer Physics*, Cornell University Press, Ithaca and London, 1st edn, 1979.
2 M. Djabourov, *Contemp. Phys.*, 1988, **29**, 273–297.
3 C. Viebke, L. Piculell and S. Nilsson, *Macromolecules*, 1994, **27**, 4160–4166.
4 M. Djabourov, J. Leblond and P. Papon, *J. Phys.*, 1988, **49**, 319–332.
5 S. Ren and C. Sorensen, *Phys. Rev. Lett.*, 1993, **70**, 1727–1730.
6 A. Parker and V. Normand, *Soft Matter*, 2010, **6**, 4916.
7 M. Rubinstein and A. V. Dobrynin, *Curr. Opin. Colloid Interface Sci.*, 1999, **4**, 83–87.
8 S. Richter, R. Matzker and K. Schröter, *Macromol. Rapid Commun.*, 2005, **26**, 1626–1632.
9 J. Hagman, N. Lorén and A.-M. Hermansson, *Biomacromolecules*, 2010, **11**, 3359–3366.
10 D. Pelc, S. Marion and M. Basletic, *Rev. Sci. Instrum.*, 2011, **82**, 5.
11 E. J. Amis, P. a. Janmey, J. D. Ferry and H. Yu, *Macromolecules*, 1983, **16**, 441–446.
12 S. Ren, W. Shi, W. Zhang and C. Sorensen, *Phys. Rev. A*, 1992, **45**, 2416–2422.
13 M. C. Blanco, D. Leisner, C. Vázquez and M. A. López-Quintela, *Langmuir*, 2000, **16**, 8585–8594.
14 M. Shibayama and M. Okamoto, *J. Chem. Phys.*, 2001, **115**, 4285.
15 M. Okamoto, T. Norisuye and M. Shibayama, *Macromolecules*, 2001, **34**, 8496–8502.
16 A. Gupta, B. Mohanty and H. B. Bohidar, *Biomacromolecules*, 2005, **6**, 1623–1627.
17 T. Matsunaga and M. Shibayama, *Phys. Rev. E: Stat., Nonlinear, Soft Matter Phys.*, 2007, **76**, 030401.
18 Y. Piñeiro, M. López-Quintela, J. Rivas and D. Leisner, *Phys. Rev. E: Stat., Nonlinear, Soft Matter Phys.*, 2009, **79**, 041409.
19 G. N. Ramachandran, *Treatise on Collagen*, Academic, New York, 1967.
20 J. Gornall and E. Terentjev, *Phys. Rev. Lett.*, 2007, **99**, 028304.
21 P. I. Rose, *Encyclopedia Polymer Science and Engineering*, John Wiley & Sons, New York, 2nd edn, 1987, vol. 7, p. 502.
22 N. R. Kubo and M. Toda, *Statistical Physics 2: Nonequilibrium Statistical Mechanics*, Springer-Verlag, 1985.
23 K. S. Cole and R. H. Cole, *J. Chem. Phys.*, 1941, **9**, 341.
24 H. B. Bohidar, S. Maity, a. Saxena and S. Jena, *Colloid Polym. Sci.*, 1998, **276**, 81–86.
25 D. Vieira, C. Avellaneda and A. Pawlicka, *Electrochim. Acta*, 2007, **53**, 1404–1408.
26 H. Walderhaug, O. Söderman and D. Topgaard, *Prog. Nucl. Magn. Reson. Spectrosc.*, 2010, **56**, 406–425.
27 E. Hahn, *Phys. Rev.*, 1950, **80**, 580–594.
28 E. O. Stejskal and J. E. Tanner, *J. Chem. Phys.*, 1965, **42**, 288.
29 S. Maity and H. Bohidar, *Phys. Rev. E: Stat., Nonlinear, Soft Matter Phys.*, 1998, **58**, 729–737.
30 J. T. Pelton and L. R. McLean, *Anal. Biochem.*, 2000, **277**, 167.
31 F. R. Brown, A. J. Hopfinger and E. R. Blout, *J. Mol. Biol.*, 1972, **63**, 101.
32 M. Muthukumar, *Adv. Chem. Phys.*, 2005, **131**, 1.
33 L. Guo, R. H. Colby, C. P. Lusignan and T. H. Whitesides, *Macromolecules*, 2003, **36**, 9999–10008.
34 L. Guo, R. H. Colby, C. P. Lusignan and A. M. Howe, *Macromolecules*, 2003, **36**, 10009–10020.
35 M. Rubinstein and A. N. Semenov, *Macromolecules*, 1998, **31**, 1386–1397.
36 W. Brown and T. Nicolai, *Colloid Polym. Sci.*, 1990, **268**, 977.
37 C. Barrera, V. Florián-Algarin, A. Acevedo and C. Rinaldi, *Soft Matter*, 2010, **6**, 3662.
38 M. Doi and S. F. Edwards, *The Theory of Polymer Dynamics*, Oxford University Press, 1986.
39 A. Kornyshev, D. Lee, S. Leikin and A. Wynveen, *Rev. Mod. Phys.*, 2007, **79**, 943–996.
40 M. Tempel, G. Isenberg and E. Sackmann, *Phys. Rev. E: Stat., Nonlinear, Soft Matter Phys.*, 1996, **54**, 1802–1810.
41 O. Lieleg, J. Kayser, G. Brambilla, L. Cipelletti and A. R. Bausch, *Nat. Mater.*, 2011, **10**, 236–242.
42 H. Tan, A. Moet, A. Hiltner and E. Baer, *Macromolecules*, 1983, **16**, 28–34.
43 H. B. Bohidar and S. S. Jena, *J. Chem. Phys.*, 1993, **98**, 3568.
44 O. Ronsin, C. Caroli and T. Baumberger, *European Physical Journal E (EPJ E), The - Soft Matter*, 2011, **34**, 1–7.

45 A. N. Semenov and M. Rubinstein, *Macromolecules*, 1998, **31**, 1373–1385.
46 F. Tanaka, *Polym. J.*, 2002, **34**, 479–509.
47 F. Tanaka, *Colloids Surf., B*, 2004, **38**, 111–114.
48 F. Tanaka, *Phys. Rev. E: Stat., Nonlinear, Soft Matter Phys.*, 2006, **73**, 061405.
49 M. A. Suarez, N. Kern, E. Pitard and W. Kob, *J. Chem. Phys.*, 2009, **130**, 194904.
50 O. Ronsin, C. Caroli and T. Baumberger, *Phys. Rev. Lett.*, 2009, **103**, 138302.
51 H. Tanaka and Y. Nishikawa, *Phys. Rev. Lett.*, 2005, **95**, 078103.
52 P. J. Lu, E. Zaccarelli, F. Ciulla, A. B. Schofield, F. Sciortino and D. a. Weitz, *Nature*, 2008, **453**, 499–503.
53 C. Patrick Royall, S. R. Williams, T. Ohtsuka and H. Tanaka, *Nat. Mater.*, 2008, **7**, 556–561.
54 A. Ron and M. Fibich, *Solid State Commun.*, 1986, **58**, 869–872.
55 R. C. Picu, *Soft Matter*, 2011, **7**, 6768.
56 C. P. Broedersz, X. Mao, T. C. Lubensky and F. C. MacKintosh, *Nat. Phys.*, 2011, **7**, 983–988.
57 C. Storm, J. J. Pastore, F. C. MacKintosh, T. C. Lubensky and P. A. Janmey, *Nature*, 2005, **435**, 191–194.